13th International Conference on
Structural Health Monitoring of Intelligent Infrastructure
DOI: 10.3217/978-3-99161-057-1-073

Insights into Rail Track Buckling from Distributed Fibre Optic Sensing Data

Neil A Hoult[1, 0000-0002-2819-7410], Fuzheng Sun[1], Liam J Butler[2, 0000-0002-2777-5952], Merrina Zhang[3]
[1] Dept of Civil Engineering, Queen's University, 58 University Ave., Kingston, ON K7L 3N6, Canada
[2] Dept of Civil Engineering, York University, 4700 Keele St., Toronto, ON M3J 1P3, Canada
[3] National Research Council of Canada, Ottawa, ON, Canada
email: neil.hoult@queensu.ca, fuzheng.sun@queensu.ca, Liam.Butler@lassonde.yorku.ca, Merrina.Zhang@nrc-cnrc.gc.ca

ABSTRACT: As climate change leads to increasing temperatures around the globe, rail track buckling has become an increasing concern for rail operators. This paper provides an overview of the key outcomes from a four-year research program that sought to explore the use of distributed fibre optic sensors (DFOS), analytical modeling, and artificial intelligence techniques to aid in track buckling assessment and detection. Lab tests and field monitoring data were used to develop and evaluate two DFOS systems, one for short length dynamic buckling assessment due to train passage and the other for long length thermal buckling assessment. The data from each system was used to develop models for the detection of buckling using different techniques depending on the quality of the initial data and the required output. Finite element model (FEM) updating and statistical FEMs were explored to predict buckling response based on measurements at service loads. Beam on elastic spring models were used to estimate the influence of train passage on buckling capacity while Gaussian process regression (GPR) techniques provided insights into buckling indicators at the field sites.

KEY WORDS: Distributed fibre optic sensing; Rail track buckling; Lab tests; Field monitoring; Data-based modelling.

1 INTRODUCTION

Continuous welded rail (CWR) is used in most modern rail networks because of the enhanced ride quality it provides as well as reducing noise and wear on the rails. However, the removal of joints along the rail means that there is no room for the rail to expand when its temperature changes relative to the rail neutral temperature (RNT) resulting in the development of a state of self-stress within the rail. If the temperature increases to a critical value, the lateral load resistance system of the rail track, consisting of ballast, ties, and fasteners, can no longer provide adequate support and the rail track buckles laterally [1,2]. The critical temperature can change over the operational life of the rail network as deterioration lowers this buckling temperature and proper maintenance increases it [1,3].

Analytical models exist to account for buckling during the design stage [1,4] however there are a number of challenges with using these models for the assessment of in-service buckling such as variations in geometry and support conditions that are present in existing rail tracks. Numerical simulations can provide more accurate estimates of track behaviour since they can account for variations in geometry and support conditions with length [2,5]. But obtaining the measurements required to develop accurate models in the field is time consuming and expensive.

Structural health monitoring techniques represent a potentially useful approach for either detecting rail track issues directly or acquiring the data required to develop more accurate models. Researchers have previously explored the use of a variety of sensors to detect rail track issues such as strain gauges [6], accelerometers [7], ultrasonic and laser vibrometers [8,9], and digital image correlation [10]. The challenge with many of these techniques is that they only provide a local measurement of rail behaviour whereas buckling can occur anywhere along the length of the rail.

A potential solution to this challenge is the use of distributed fibre optic sensors (DFOS). For strain sensing, research has focused on the use of Rayleigh based systems when high-resolution (gauges lengths less than 1 mm are possible) and high-accuracy measurements (up to $\pm$ 1 microstrain at the fiber core for Rayleigh based systems) are required [11]. And Brillouin based systems when lower resolution (gauge lengths of 50 mm) and lower accuracy ($\pm$ 15 microstrain) [12] is an acceptable trade-off to achieve longer sensing lengths (100 m per channel for Rayleigh-based systems [11] versus up to 25 km and more for Brillouin-based systems [12]). Most of the current research using DFOS for rail applications has focused on the response of the rail due to vehicle loading [13,14]. Initial studies have been conducted on short lengths of rail to measure thermal strain due to free expansion using Brillouin Optical Time Domain Analysis (BOTDA) [15,16] as well as to measure strains due to thermal stress in the lab and the field [16].

The goal of the research campaign described in this paper was to evaluate the viability of using DFOS for the assessment of rail track buckling. The objective of this paper is to provide an overview of the entire research campaign starting with lab-based thermal buckling experiments that were used to update finite element models (FEM) as well as to explore the use of statistical FEM (StatFEM) with distributed sensing data for the first time. Three field tests were also undertaken on a tangent track and a curved track section in Ontario, Canada to acquire first of their kind data sets and to explore the use of DFOS data to inform improved models of rail track buckling.

2 LAB TESTING

2.1 Introduction

Before undertaking field tests, the first phase of this research involved a series of small-scale lab-based experiments to

DOI: 10.3217/978-3-99161-057-1-073

explore the use of both Optical Frequency Domian Reflectometry (OFDR), and BOTDA measurements for assessing rail track buckling. The rails were subjected to both mechanical and thermal loading to induce buckling in the rail.

2.2 Specimens

An ASCE 5.95 kg/m (12 lbs/yd) mining rail specimen with the length of 3,048 mm (Hammer Steel Products, Canada) was used, as buckling of the member could be induced within the available lab constraints. The specimen had a specified elastic modulus (E) of 207 GPa, cross-sectional area (A) of 761 mm^2, and coefficient of thermal expansion (α) of 11.6 × 10-6 / ℃. The second moment of area was 53,000 mm^4 about the weak axis (I_y) and 229,000 mm^4 about the strong axis (Ix). The specimen was instrumented with eight nylon-coated single mode strain measurement optical fibres (F1 – F8) to measure the surface strain and a temperature measurement fibre to measure the distributed temperature as illustrated in Fig. 1. Further details about the specimens are provided in [17,18].

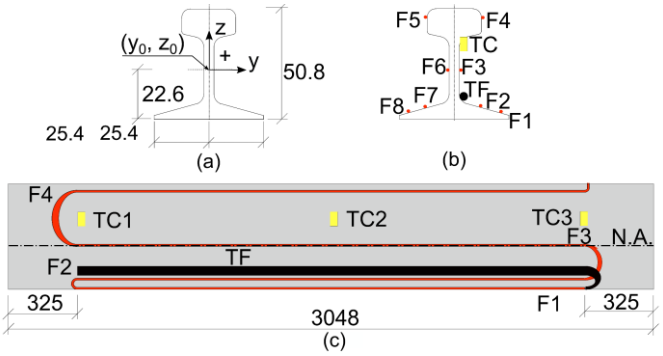

Figure 1. Lab buckling test specimen (in mm). (a) rail cross-section dimensions, (b) fibre locations on cross-section, (c) longitudinal dimensions and fibre layout.

2.3 Test setup

As shown in Figure 2, the testing frame consisted of two steel plates that were connected to four threaded rods using nuts. Two types of tests were conducted: (1) buckling due to applied load from an actuator with three different lateral support conditions and (2) thermal buckling caused by restraining axial elongation due to changes in temperature.

Figure 2(a) shows the schematic frame setup for the applied load buckling with no lateral restraint (NS) and thermal buckling tests. In the applied load tests with lateral restraint, the lateral restraint was provided by springs with a stiffness of 32.7 N/mm, and a maximum compressible length of 30.2 mm. Figure 2(b) illustrates the test setup for the applied load tests with one spring placed at the mid-length test, and Figure 2(c) shows the applied tests with two springs placed at 1/3 and 2/3 of the rail length, respectively, where weak-axis buckling occurs in the vertical direction.

For the thermal buckling tests, the rail temperature was adjusted by changing the temperature within a climate chamber where the specimen was placed. The steel frame experienced similar thermal expansion/contraction as the rail due to a temperature increase/decrease (ΔT), so to keep the length of the rail constant (e.g. full axial restraint), an axial load was applied to the rail to ensure the net axial displacement of the rail was 0 mm. For all tests, the axial load was applied by a hydraulic jack with a capacity of 1010 kN and measured using a load cell with a 222 kN capacity. The actuator, supports, and the specimen could not be aligned perfectly, and axial loads with different eccentricities occurred in all tests. A linear potentiometer (LP) was placed at the mid-length of the rail to measure the lateral deflection during the test. The strain was measured using a LUNA ODiSI 6104 analyzer (LUNA Innovation, USA) for the OFDR tests and an NBX-6050A Brillouin Optical Time Domain Analysis (BOTDA) analyzer (Neubrex, Japan) for the BOTDA tests.

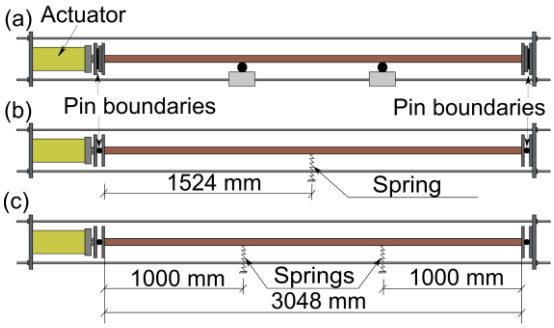

Figure 2. Lab buckling test setup. (a) no lateral restraint, (b) one spring, (c) two springs.

2.4 Results

The lab experiments were used to evaluate the potential for using DFOS measurements to assess buckling. Because 8 fibres were placed around the rail cross-section (see Figure 1), it was possible to define a fitted strain plane using the measurements at each point along the length of the rail as seen in Figure 3.

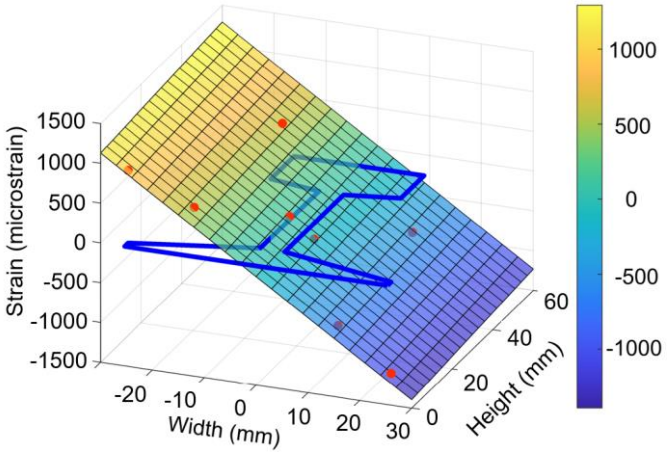

Figure 3. Strain measurements from 8 fibres on the rail forming a strain plane enabling calculation of axial strain and strong and weak axis curvature.

The strain plane seen in Figure 3 can be used to calculate the axial strain and weak and strong axis curvatures in the rail. The curvatures can then be numerically integrated twice to obtain a lateral deflection profile along the rail. One of the key conclusions from this part of the research was that both OFDR and BOTDA sensor systems could be used to measure the response of the rail using the strain plane approach although OFDR provided more accurate measurements, especially of the lateral restraint force provided by the springs [18]. While measurements of axial strain and displacement can be used as

DOI: 10.3217/978-3-99161-057-1-073

thresholds for assessing the impact of buckling, to provide predictions of future behaviour, a numerical model based on the experimental data is required as discussed in the next sections. Further details about the lab-based experimental campaigns can be found in [17,18].

2.5 Finite element model updating

One challenge with using monitoring data to estimate the ultimate limit state behaviours of a structure is that the data is usually recorded at service loads. In this investigation DFOS data captured at service loads (i.e., applied loads and temperatures that were 50% of ultimate) were used to update finite element models to estimate the buckling capacity. A commercially available finite element analysis (FEA) program (i.e., Abaqus) was used to model the tests. The 3.048 m long slender member was modelled with 30 three-noded beam elements (B32), with the same cross-sectional and material properties as the rail. Connector elements with one degree of freedom perpendicular to the member were used to model the spring supports and were given one of two stiffnesses: (i) the manufacturer specified value (i.e., 32.7 N/mm) or (ii) the stiffness calculated from the DFOS measurement derived reaction force divided by the DFOS measurement derived displacement at the support location for each test [18]. Three steps of analyses were undertaken: 1. a linear buckling analysis to obtain the initial deflected shape, 2. a static general analysis considering geometric nonlinearity to determine the value of the mid-span imperfection and the end eccentricities through model updating and, 3. a static risk analysis to develop the buckling load-displacement response. Two approaches were taken to step 2: (a) a coarse grid and (b) a fine grid analysis. In the coarse grid analysis, the initial eccentricity parameters (at the supports and at midspan) were varied over a range of ±2.0 mm with an increment of 0.5 mm and the optimum analysis was chosen based on the computed root mean square error (RMSE) between the modelled curvature values and the measured curvature values. In the fine grid analysis, each of the optimal eccentricity values from the coarse grid analysis were varied over a range of ±0.5 mm with an increment 0.1 mm resulting in 1331 analyses.

Figure 4 presents the load-deflection responses from the finite element model updating investigation for (a) the NS tests and (b) the OS tests. Also plotted in the figure are the measured load and displacement at each load stage. Figure 4(a) shows the results from the tests using both the OFDR and BOTDA sensing systems. The difference in behaviour between the OFDR and BOTDA tests is not a function of the measurement systems but is due to the different axial load eccentricities present in each test. The results from the fine and coarse grid approaches plot on top of each other suggesting either approach to estimating the impact of eccentricities on the tests results is acceptable. Overall, the finite element model updated using the service load data was able to capture the ultimate behaviour of the rail accurately. In Figure 4(b) it can be seen that using the manufacturer or estimated spring stiffness provides the same result for the OFDR system.. This is because the higher spatial resolution and accuracy of this system compared to the BOTDA allows for localized behaviour, such as lateral supports, to be resolved more accurately. Using the manufacturer's spring stiffness along with the BOTDA data at service loads enables the updated FEM to capture the full behaviour. Though the estimated spring stiffness model is not as accurate, it is still conservative.

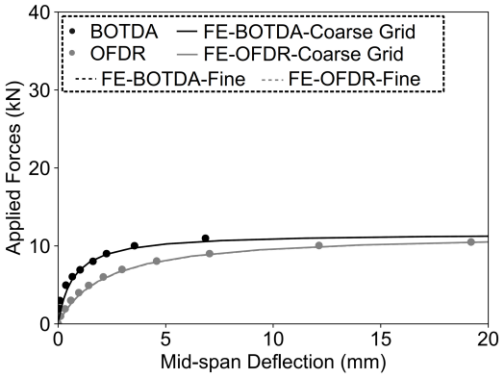

(a) No lateral restraint tests comparing BOTDA and OFDR data to FE models using Coarse and Fine Grid approach

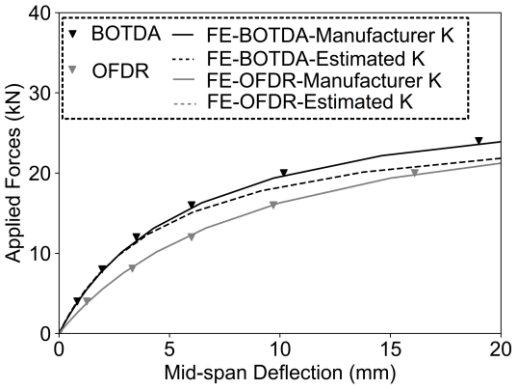

(b) One spring restraint tests comparing BOTDA and OFDR data to FE models using both the Manufacturer and Estimated spring stiffness, K, from the data

Figure 4. FE model updating results compared to measured response from applied load tests.

2.6 Statistical FEM model

The previous section highlighted that DFOS data could be used to support FEM updating but one limitation of the approach is that depending on the number of structural parameters to be optimized and the complexity of the model, model updating can have a high computational cost associated with finding the structural parameters that provide the optimum fit to the data. A second limitation is that traditional model updating assumes the model perfectly represents the true structural response whereas in reality the model always involves assumptions and idealization of the actual system (e.g., materials, boundary conditions, loading, etc.). To address these two limitations, a second FEM updating investigation was undertaken, exploring the use of the Statistical FEM (StatFEM) with distributed sensor data for the first time [19]. The basis of the StatFEM approach is that the measured structure response is composed of the true structure response and errors due to sensor measurement noise that have a known statistical distribution. The true structural response is assumed to be a combination of the FEM structural response and the model-reality mismatch due to model idealization and assumptions. The same approach was taken whereby data acquired at service

DOI: 10.3217/978-3-99161-057-1-073

loads was used to update the model that was then used to predict ultimate capacity. In this investigation, polynomial chaos expansion (PCE) was investigated as an approach to generate the FE probability distribution prior to updating as opposed to the more traditional Monte Carlo simulation. This resulted in order of magnitude improvements in computation time from 16 hours and 40 minutes to 9 minutes with a less than 1% reduction in accuracy.

Figure 5 shows the strain versus load relationship for an (a) OFDR tests and (b) a BOTDA test for when 40 data points along the rail length (i.e. $n_y = 40$) were used. It can be seen that the initial FE probability distribution overestimated the strain at a given load in the nonlinear range but that the StatFEM prediction of the ultimate limit state response incorporating the DFOS data collected in the service load range shows an excellent visual agreement with the measured ultimate limit state structural response. The model updated using the OFDR measurements (Figure 5(a)) demonstrates an excellent fit to the data over the entire measurement range and the error range (the grey shaded area) is smaller than the model updated using BOTDA data (Figure 5(b)).

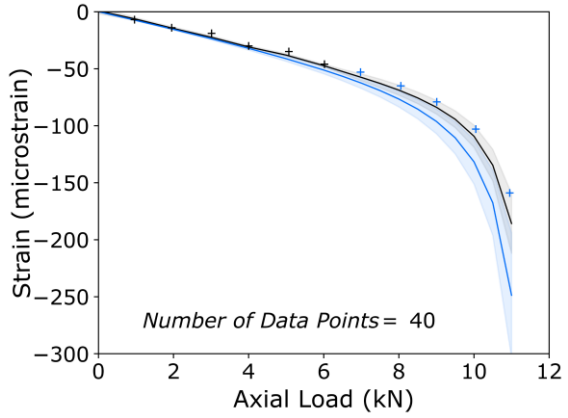

(a) OFDR measurements

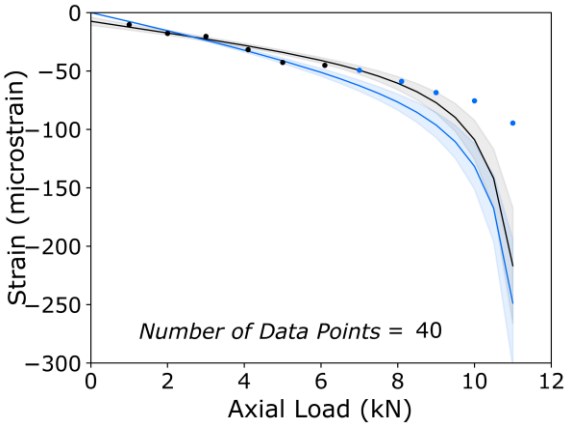

(b) BOTDA measurements

Figure 5. Strain versus load relationship where the blue line and shaded area represents the FE prediction, the black line and shaded area represent the StatFEM prediction, and the discrete points are measured strain.

The number of data points used to update the model was also found to play an important role in terms of prediction accuracy and the size of the error envelope. This shows the benefit of using DFOS for FEM updating as the number of points enable much higher prediction accuracy. Further details on the use of DFOS with the StatFEM can be found in [19].

3 FIELD MONITORING

3.1 Introduction

Having demonstrated the potential to use DFOS for monitoring of thermal buckling and development of robust numerical models using controlled lab-based experiments, the next phase of the research involved three separate field investigations to evaluate the use of DFOS to monitor rail track buckling in the field: (i) short term dynamic monitoring, (ii) long-term thermal monitoring and assessment of tangent track, and (iii) long-term thermal monitoring and assessment of curved track.

3.2 Site installations

The site installations were similar in that three nylon-coated strain measurement fibres with a diameter of 0.9 mm were installed at the various heights in the cross section as illustrated in Figure 7 so that the strain plane in Figure 3 could be measured. The two long-term monitoring installations were similar with the major difference being one was on a tangent track and the other was on a curved track. In both cases, a 20 m long 8 mm diameter temperature fibre and 4 thermocouples were also installed on the rail as shown in Figure 7 to capture thermal effects. The long-term fibre optic data was acquired using an NBX-6050A Brillouin Optical Time Domain Analysis (BOTDA) analyzer with readings being taken every 30 minutes over the course of one month [20]. For the short-term dynamic monitoring, the installed fibre length was 9 m (as opposed to the 20 m shown in Figure 7) so that the data could be acquired at a rate of 13 Hz using a LUNA ODiSI 6104 analyzer [21].

DOI: 10.3217/978-3-99161-057-1-073

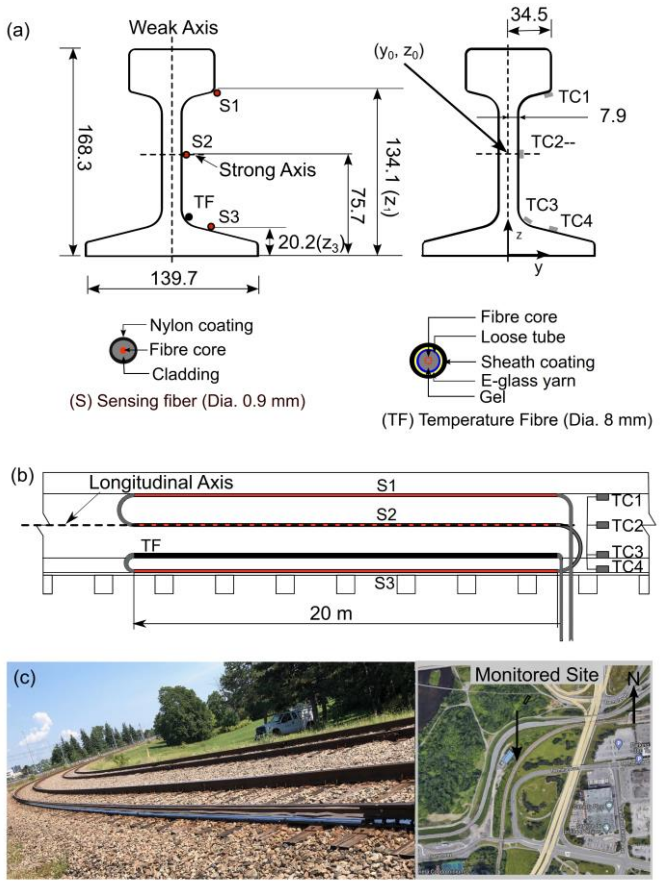

Figure 7. Field monitoring installation on curved track. Strain (S) and temperature fibre (TF), and thermocouple (TC) locations on (a) cross-section (in mm) and (b) rail length, and (c) site layout and location.

3.3 Impact of temperature and train passage

One of the key findings from the installation on the tangent track was that solar gain had an impact on rail strain measurements. Figure 8 shows the difference in temperature measurements from the thermocouples at various points on the rail cross-section relative to the location of the temperature fibre (TC3). It can be seen that at night (between midnight and 8 am in Figure 8) the difference in temperature measurements is less than 1°C and is within the noise of the thermocouple measurements. During the day this difference can be as high as approximately 2°C and depends on the position of the sun relative to the rail as well as the amount of cloud cover. The impact of this temperature difference is three-fold. First, it challenges the conventional assumption of constant temperature in the rail cross-section often used in buckling assessment. Second, the strain measurements from the fibres must be compensated for temperature with the correction factor being approximately 20 microstrain/°C for the BOTDA system [16]. Third, this differential temperature can cause rail bending if the rail is not adequately restrained, which could increase the likelihood of rail track buckling.

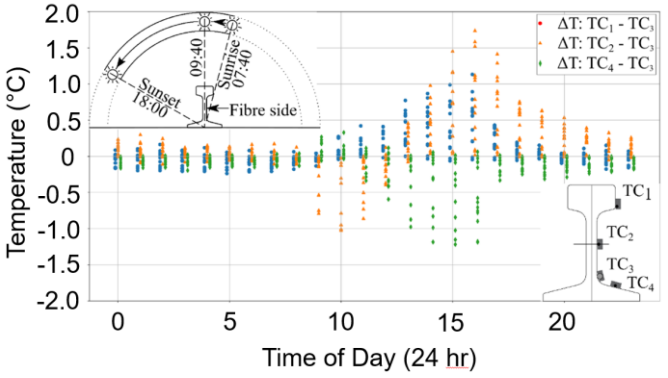

Figure 8. Difference in rail temperature at 4 different locations on the rail cross-section with time of day.

A second issue that affects the accuracy of long-term monitoring data is the passage of trains. Figure 9 shows three sets of consecutive measurements taken at the curved track site taken before any trains passed, after the position of Train 1, and after the passage of Train 2 at a constant temperature.

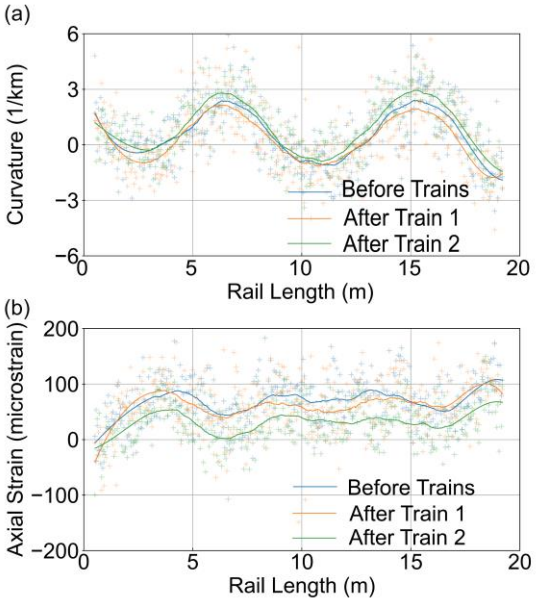

Figure 9. Effect of train passage on DFOS measurements at the curved rail site. (a) Curvature and (b) Axial Strain

One can see from Figure 9 that both the curvature and the axial strain are impacted by the passage of a train. While this might not be the case for a track that was properly restrained against lateral and longitudinal movement, previous research has demonstrated that rail tracks supported by wooden ties and gravel ballast can experience longitudinal movement and thus changes in axial strain due to the passage of trains [22]. Thus, when monitoring and assessing rail tracks for buckling using DFOS, temperature effects due to solar gain and the passage of trains are important issues that must be carefully addressed. In the case of thermal effects, a potentially straightforward solution is to use combined strain and thermal measurement fibres at all three measurement heights along the rail.

3.4 Dynamic thermal buckling models

Dynamic buckling occurs when the train wheel loads acting on the rail track cause a section of the track to lift off the ties and

DOI: 10.3217/978-3-99161-057-1-073

become laterally unsupported. If that section of rail track is already prone to buckling due to being on a curve, having a small amount of misalignment along its length, or both then railway buckling can occur at lower temperatures than static thermal buckling.

DFOS measurements were taken with the OFDR analyser along a section of curved track as a passenger train travelled over the instrumented section. Because strains were measured at multiple heights on the rail, the curvature profile along the instrumented section could be derived. A beam on elastic foundation (BOEF) model, where the rail is modelled as a beam with the same flexural stiffness (EI) as the rail and the foundation is modelled as a series of elastic springs, was then created. The curvature pattern was then used to update the BOEF model to estimate the track modulus by adjusting the spring stiffness until the measured rail curvature matched the model beam curvature, which resulted in a track modulus of 13.6 MPa in this case.

To predict the dynamic buckling temperature, a finite element model was constructed in ABAQUS using two-noded beam elements. Two types of connector elements were used in the FE model to simulate the interaction between the rail track and the rail ties as well as between the ties and the ballast, respectively. The track modulus that affects the rail lifting-off behavior under train loading was derived from the DFOS measurements as noted above and the rest of the structural parameters that affect static thermal buckling behavior were obtained from the literature [21]. The FE modelling was conducted in two stages. First, a static nonlinear analysis was conducted to get the railway lift-off response under train loading. Afterwards, the impact of railway lift-off response on the lateral resistance provided by the ballast to the railway system was inputted into the railway FE model to simulate the railway dynamic buckling. A misalignment in the rail of either 20 mm or 34 mm was modelled and then an increasing temperature was applied to the model to determine the temperature increase above the rail neutral temperature versus lateral displacement response as seen in Figure 10. Further details of the model can be found in [21].

From Figure 10 it can be seen that the passenger cars had no impact on the buckling behaviour as the dynamic buckling curve for the passenger cars plots on top of the static thermal buckling curve. This was because the rail passenger cars were not heavy enough to cause the rail to lift off the ties and reduce the lateral resistance. The locomotives, on the other hand, were heavy enough to cause the track between trucks of the locomotive to lift off the ties. As a result, the temperature to cause thermal buckling while a locomotive is passing was found to be lower than the static case. By comparing Figures 10(a) and 10(b) one can also see that rail misalignment impacts both the static and dynamic buckling temperature where larger misalignments lead to lower critical buckling temperatures as would be expected. The combined effect of dynamic buckling and misalignment can be significant since in this case the critical temperature increase to cause buckling went from 42.6°C with a 20 mm misalignment and no train loading to 35.3°C with a 34 mm misalignment and locomotive loading.

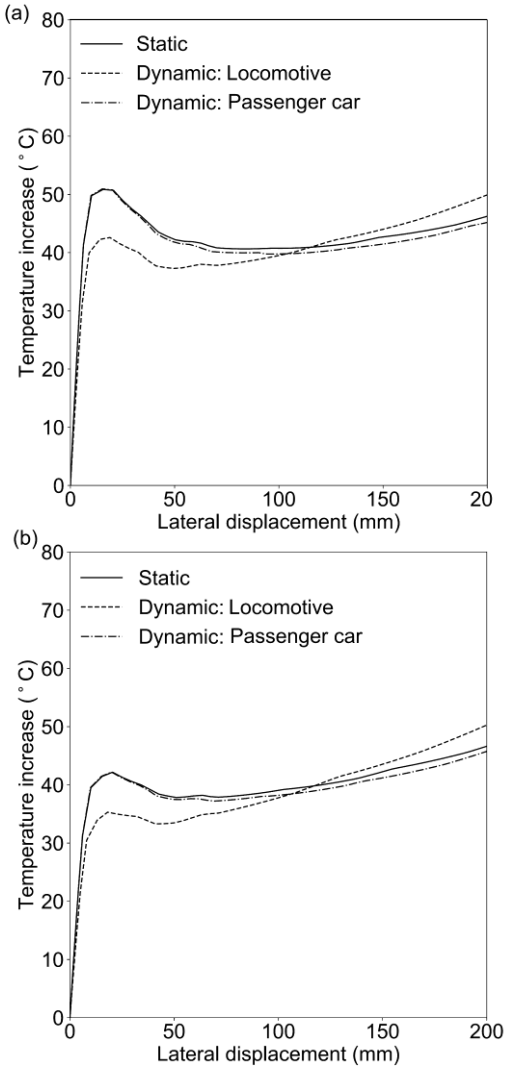

Figure 10. Static versus dynamic buckling response for monitored section of track. (a) 20 mm misalignment, (b) 34 mm misalignment

3.5 Data-driven thermal buckling models

In many infrastructure monitoring applications, the system being monitored is too complex to be accurately captured by a physics-based model. Such is the case for many rail buckling applications where the likelihood of buckling is a function of a complex system that involves interaction between the environment and a physical system with spatial varying geometric and material properties. As noted earlier in the paper, the position of the sun and cloud conditions affect the rail temperature and due to the lack of perfect rail restraint (e.g., due to gaps between the restraint plates and the rail) the rail experiences changes in the stress-state due to the passage of trains. Other issues such as variable support stiffness and rail track alignment further complicate the situation and make it essentially impossible to develop a comprehensive physics-based model.

One potential solution to this is to use a data-driven modelling approach. DFOS produces thousands of data points along the length of the rail to capture the spatial variability in both strain and temperature and allows for scans to be taken multiple times a day over the course of weeks to help resolve

DOI: 10.3217/978-3-99161-057-1-073

the temporal variability. Gaussian process regression is a data-regression technique that allows for the uncertainty of the model to be calculated. The first step in the process is to select an appropriate kernel which defines the function and the relationships between variables. In the current work a Matern32 + linear kernel was selected based on a comparison of 12 different kernels to determine which one best fit the data. Each of the 12 models was trained using the first two weeks of data from the curved track monitoring site and then were used to predict the data from the last two weeks of monitoring.

Two different GPR models were developed: Model 1 defined a relationship between the axial strain and curvature along the rail and the input variables of rail surface temperature and location. Model 2 also considered train passage and non-uniform rail surface temperature as noise components that could impact the results based on the observations presented earlier. Figure 11 presents the GPR model results for axial strain versus temperature where the blue line represents the most likely relationship proposed by both models. The dark blue shaded region in the figure is the range of potential relationships according to Model 1 while the light blue region is the range of potential solutions for Model 2. It should be noted that the associated uncertainty for each model represents the range of potential models and should not be confused with other potential sources of error such as measurement error. If enough training data was available, it would be possible to have a GPR model with no uncertainty, but the actual measurements might not lie on the curve due to measurement noise. More details about the development of the models can be found in [20].

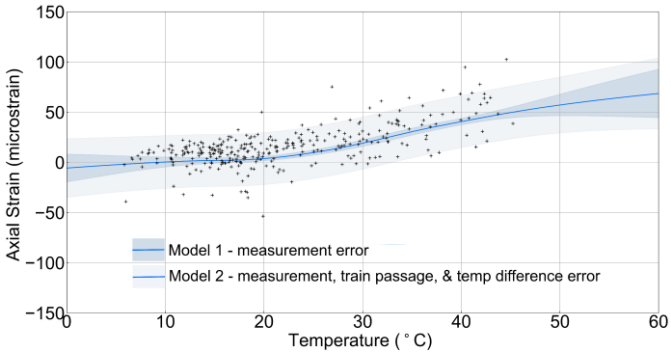

Figure 11. GPR model of the relationship between axial strain and temperature with and without consideration of train passage and differential rail temperature effects.

From Figure 11 it can be seen that the uncertainty band for Model 1 is smaller than for Model 2, due to the added potential uncertainty due to train passage and temperature variation around the cross-section of the rail. The uncertainty is also higher when the temperature is below approximately 7°C and above 45°C due to lack of training data in these regions. This presents a challenge as rail operators are most concerned about the behaviour above 40°C but there is inherently going to be less or even no training data at these critical temperature levels. Another important thing to note about Figure 11 is that many of the measured points do not match the proposed relationship or in some cases do not even fall within the uncertainty bounds. One reason for this is measurement error but there is another more fundamental issue and that is for this system there is more than one state of stress that can occur at a given temperature. Because of variables such as gaps between the rail and the supports, train passage, and differential rail temperatures, the rail can actually take on a variety of positions at a given temperature. As such, a limitation of using GPR for systems such as these is that they are not accurately described by a closed-form solution. However, they do provide rail operators with guidance as to the overall relationship.

3.6 Future Work and Scalability

The initial results suggest that DFOS show promise as a rail track thermal buckling detection tool. However, three major issues still need to be addressed: (i) installation, (ii) improved thermal compensation, (iii) and automated detection. In terms of the installation, in a parallel study the research team developed a prototype robotic system that could install the fibre optic cables at various heights on the rail section an order of magnitude faster than human installers with improved placement accuracy. In the current work, temperature was only measured along the rail at one location on the cross-section, which meant that temperatures at other locations must be inferred from the single fibre optic measurement and thermocouple measurements. However, there are commercially available fibres that combine strain and temperature measurement fibres in a single housing that could be used to improve the temperature compensation. Finally, while the current research has shown that data driven techniques can be used to assist in modelling rail behaviour, further work is required to develop models and detection techniques that can be used by rail operators to automatically detect and provide warnings of thermal rail track buckling.

4 CONCLUSIONS

This paper presented the key findings from a four-year investigation into the use of distributed fibre optic sensing (DFOS) to support the monitoring and assessment of rail tracks that are susceptible to thermal buckling. The key conclusions include:

1. Installing three DFOS strain sensing fibres on the cross-section of the rail allows a strain plane at every sensor location along the length to be derived. Axial strain, and weak and strong axis curvature can then be determined and the curvature can be numerically integrated to obtain displacement along the length of the rail.
2. DFOS data can be used to update finite element models that are capable of predicting the ultimate response even when model updating is based on data acquired at service loads. Additionally, DFOS data can be used with the StatFEM to provide not only more accurate models but also error bounds associated with sensor noise.
3. The change in strains due to the passage of trains and due to variable heating of the rail cross-section due to solar effects are two of the challenges associated with using DFOS results for the assessment and modeling of buckling behaviour.
4. Dynamic DFOS measurements can be used with a beam on elastic foundation (BOEF) model to estimate the deflected shape of the rail and the track modulus. The deflected shape and track modulus can then be used in an FE model of the rail track to estimate the impact of vehicle load on the dynamic thermal buckling behaviour.

DOI: 10.3217/978-3-99161-057-1-073

5. Data-driven models such as Gaussian process regression (GPR) offer a potential approach for developing models in situations where a physics-based model is intractable. However, if the system does not have a unique solution at a given temperature, e.g., due to poorly constrained degrees of freedom from gaps between the rail and sleepers, the GPR model may not capture this behaviour but can still serve as a guide for rail network managers.

ACKNOWLEDGMENTS

This project was supported in part by collaborative research funding from the National Research Council of Canada's Artificial Intelligence for Logistics Program, and the Natural Sciences and Engineering Research Council of Canada. The authors would also like to acknowledge the support of Paul Montgomery and Andrew MacDonald from City of Ottawa in providing temporary access for placing the BOTDA analyzer, Paul Charbachi from VIA Rail Canada Inc., in assisting with coordinating field tests, and Heshan Fernando from Queen's University for assisting with the field tests. And finally the support of Fehmi Cirak of the University of Cambridge and Eky Febrianto of the University of Glasgow for their assistance with the StatFEM portion of the research.

REFERENCES

[1] Kish A, Samavedam G. Track buckling prevention: theory, safety concepts, and applications. John A. Volpe National Transportation Systems Center (US); Report for the US Department of Transportation. Report no. DOT/FRA/ORD-13/16. 2013.
[2] Pucillo GP. Thermal buckling and post-buckling behaviour of continuous welded rail track. Vehicle System Dynamics. 2016; 54(12): 1785-1807.
[3] Ngamkhanong C, Feng B, Tutumluer E, Hashash YMA, Kaewunruen S. Evaluation of lateral stability of railway tracks due to ballast degradation. Construction and Building Materials. 2021; 278: 122342.
[4] Kerr AD. An improved analysis for thermal track buckling. International Journal of Non-Linear Mechanics. 1980; 15(2): 99-114.
[5] Lim N-H, Park N-H, Kang Y-J. Stability of continuous welded rail track. Computers & Structures. 2003; 81(22-23): 2219-2236.
[6] Tam HY, Lee T, Ho SL, Haber T, Graver T, Méndez A. Utilization of fiber optic Bragg Grating sensing systems for health monitoring in railway applications. Structural Health Monitoring. 2007; 2: 1824-1831.
[7] Mori H, Tsunashima H, Kojima T, Matsumoto A, Mizuma T. Condition Monitoring of Railway Track Using In-service Vehicle. Journal of Mechanical Systems for Transportation and Logistics. 2010; 3(1): 154-165.
[8] Vangi D, Virga A. A practical application of ultrasonic thermal stress monitoring in continuous welded rails. Experimental Mechanics. 2007 Oct; 47: 617-623.
[9] Damljanović V, Weaver RL. Laser vibrometry technique for measurement of contained stress in railroad rail. Journal of sound and vibration. 2005; 282(1-2): 341-366.
[10] Le Pen L, Watson G, Powrie W, Yeo G, Weston P, Roberts C. The behaviour of railway level crossings: Insights through field monitoring. Transportation Geotechnics. 2014; 1(4): 201-213.
[11] Luna Innovations (2024) ODiSI 7100 Series data sheet Available from: https://lunainc.com/sites/default/files/assets/files/data-sheets/ODiSI%207100%20Data%20Sheet%20oct2023a_CVS.pdf. Date accessed: August 16, 2024.
[12] Neubrex. Neubrescope NBX-6026/NBX-6056 2018. Available from: https://www.neubrex.com/pdf/NBX_6026&6056.pdf. Date accessed: July 23, 2023
[13] Minardo A, Porcaro G, Giannetta D, Bernini R, Zeni L. Real-time monitoring of railway traffic using slope-assisted Brillouin distributed sensors. Appl Opt. 2013; 52(16): 3770-3776.
[14] Wheeler LN, Take WA, Hoult NA, Le H. Use of fiber optic sensing to measure distributed rail strains and determine rail seat forces under a moving train. Canadian Geotechnical Journal. 2019; 56(1): 1-13.
[15] Gu L, Zhang L, Bao X, Zhang M, Zhang C, Dong Y. Detection of Thermal Strain in Steel Rails with BOTDA. Applied Sciences. 2018; 8(11): 2013.
[16] Barker C, Hoult NA, Zhang M. Development of an axial strain measurement system for rails. Journal of Performance of Constructed Facilities. 2021; 35(1): 04020145.
[17] Sun, F., Hoult, N.A., Butler, L.J. et al. Distributed monitoring of rail lateral buckling under axial loading. J Civil Struct Health Monit 12, 757–774 (2022).
[18] Sun, F., Hoult, N. A., Butler, L., & Zhang, M. (2024). Monitoring and assessment of buckling in slender members with varying lateral restraint and thermal loading using distributed sensing. *Journal of Structural Engineering*, *150*(1), 04023190.
[19] Sun, F., Febrianto, E., Fernando, H., Butler, L. J., Cirak, F., & Hoult, N. A. (2023). Data-informed statistical finite element analysis of rail buckling. *Computers & Structures*, *289*, 107163.
[20] Sun, F., Hoult, N. A., Butler, L. J., & Zhang, M. (2024). Field monitoring and prediction of the thermal response of an in-service curved continuous welded rail using distributed fiber optic strain measurements. *Journal of Civil Structural Health Monitoring*, 1-15.
[21] Sun, F., Hoult, N. A., Butler, L., & Zhang, M. (2024). Dynamic Monitoring of Rail Behavior under Passenger Train Loading Using Distributed Fiber Optic Sensors. *Journal of Performance of Constructed Facilities*, *38*(4), 04024018.
[22] Murray, C. A., Take, W. A., & Hoult, N. A. (2015). Measurement of vertical and longitudinal rail displacements using digital image correlation. *Canadian Geotechnical Journal*, *52*(2), 141-155.